Supplementary information

Scalable synthesis of Bi_2O_2S nanoplates with large piezoelectric potential induced by built-in electric field in $[Bi_2O_2]^{2+}$ layer for degradation of organic dyes

Zhende Wu,‡ Jing Xie*,‡ Suixin Yin, Zhenjiang Lu, Jindou Hu, Yali Cao*

State Key Laboratory of Chemistry and Utilization of Carbon Based Energy Resources, College of Chemistry, Xinjiang University, Urumqi, 830046, Xinjiang, PR China.

*Corresponding author. Tel: +86-991-8583083; Fax: +86-991-8588883; Email: caoyali523@163.com (Y. Cao); xiejing@xju.edu.cn (J. Xie).

‡ Authors with equal contributions to this work.

Experimental section

S1. Chemicals

Bismuth nitrate ($Bi(NO_3)_3 \cdot 5H_2O$, Aladdin Reagent Shanghai Co., Ltd.), sodium hydroxide (NaOH, Tianjin Xinbote Chemical Co., Ltd.), sublimated sulfur (S, Tianjin Best Chemical Co., Ltd.), precipitated sulfur (S, Tianjin Best Chemical Co., Ltd.), thioacetamide (C_2H_5NS, Aladdin Reagent Shanghai Co., Ltd.), and thiourea (CH_4N_2S, Aladdin Reagent Shanghai Co., Ltd.) were all commercially available analytically pure reagents in the experiment.

S2. Synthesis of Bi_2O_2S nanosheets

Bi_2O_2S was synthesized via a low-heating solid-state chemical method. 4 mmol $Bi(NO_3)_3 \cdot 5H_2O$ and 40 mmol NaOH were ground into powder, then the two compounds were mixed and ground until the reaction system turned yellow. 2 mmol of thiourea was added and ground for about 30 min until the reaction system turned dark red. The resulting mixture was sealed and placed in a conical flask, then placed in a water bath at 80℃ for 12 h. Finally, the mixture was filtered and washed with distilled water, and the product was collected after drying and labeled as "BOS-S".

Other samples were fabricated with the same procedure except for the thiourea was replaced by thioacetamide, precipitated sulfur and sublimated sulfur, the corresponding products were labeled as "BOS-T", "BOS-C" and "BOS-H", respectively.

S3. Characterization of piezocatalysts

The morphology was observed by field emission scanning electron microscopy (FESEM, Hitachi S-4800H) using an accelerating voltage of 5 kV, transmission electron microscopy (TEM, Hitachi H-600) using an accelerating voltage of 120 kV, and high-resolution transmission electron microscopy (HR-TEM, JEOL JEM-2010F) using an accelerating voltage of 200 kV. The element component was measured by the energy disperse X-ray spectrum (EDS, EDAXTLS). The crystallographic information of samples was investigated by performing X-ray powder diffraction (XRD) characterization using a D8 Advance X-ray diffractometer with non-monochromated

Cu Kα X-ray source (λ=1.054056 Å) in an operating voltage of 40 kV and a beam current of 40 mA. X-ray photoelectron spectroscopy (XPS) (Thermo Fisher Scientific ESCALAB250Xi) employing Al Kα (1486.6 eV) was taken to identify the surface components and valence states of products. Hydroxyl (·OH) and super-oxide ($\cdot O_2^-$) radicals were measured on electron spin resonance (ESR) spectrometer (MEX-nano, Bruker) via 5, 5-dimethyl-1-pyrroline N-oxide (DMPO). The optical properties and energy band structure of the samples were tested by UV-vis Diffuse Reflectance Spectroscopy (UV-vis, DRS). The piezoelectric properties were determined by piezo-response force microscopy (PFM, Bruker, ICON). Piezoelectric constants (d33) were calculated from the amplitude-voltage butterfly loops.

S4. Piezocatalytic performances measurements

A customized piezoelectric ultrasonic machine at 100 W, 40 kHz was used as the vibrational excitation source. The simulated pollutants chosen for this experiment were rhodamine B (RhB), tetracycline hydrochloride (TCH), methylene blue (MB), and methyl orange (MO). The volume of organic pollutants was 100 mL, the concentration of RhB, MB and MO were 5 mg L^{-1}, the concentration of TCH was 10 mg L^{-1}, and the amount of catalyst was 30 mg. The specific operation steps are as follows: the catalyst was dispersed in RhB (or TCH, MB, MO) solution, the system was stirred in the dark for 30 min before ultrasound to reach the physical adsorption-desorption equilibrium. In order to avoid the influence of high temperature on the piezoelectric catalytic performance, the water should be changed every 10 min. 4 mL of the pollutants were taken at fixed interval and centrifuged at high speed (8000 r/min, 5 min) to remove catalyst, the absorbance of the supernatant should be determined by UV-vis absorption photometer.

In addition, various scavengers were employed to elucidate the roles of different reactive species in the degradation process. p-Benzoquinone (BQ), isopropanol (IPA), triethanolamine (TEOA) and silver nitrate ($AgNO_3$) were used as the trapping agents for $\cdot O_2^-$ radicals, ·OH radicals, h^+ and e^-, respectively. At the end of the dark reaction experiment, 10 mL of the radical trapping agent with the concentration of 1 mmol L^{-1} was added into the catalytic reaction system, then the performance test was carried out.

S5. The calculation of piezoelectric coefficient (d_{33})

The d_{33} values could be acquired through calculating the corresponding slope of the Displacement-Voltage curve according to Equation:

$$d_{33} = (A-A_0)/(V-V_0)$$

Where V and A represent the applied voltage and amplitude respectively; V_0 and A_0 are the intersection point of the amplitude butterfly loop curve.

Supplementary Figs and Tables

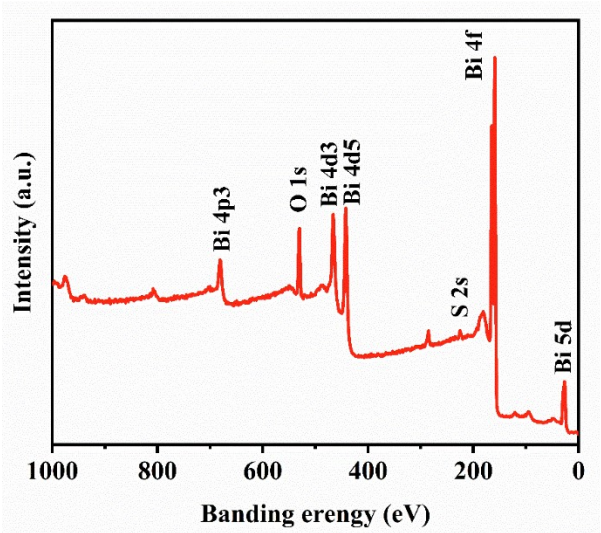

Fig. S1 XPS survey spectra of BOS-S.

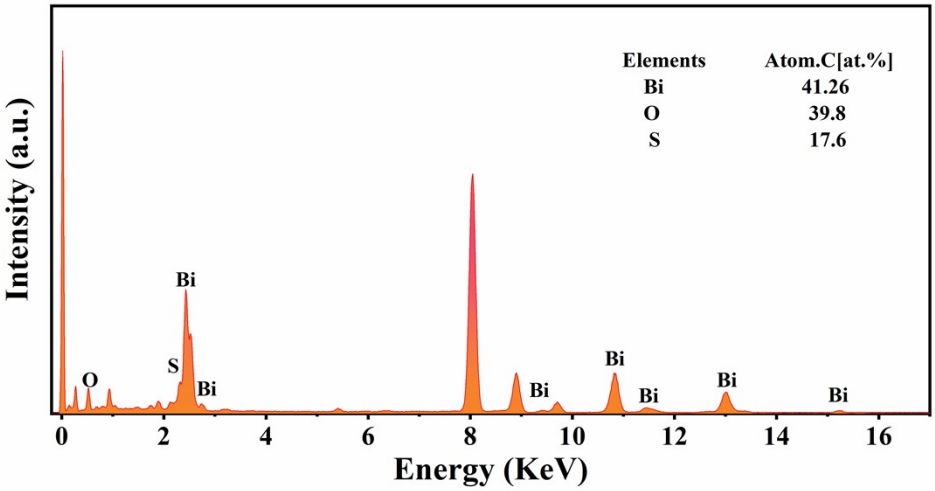

Fig. S2 EDS spectrum of BOS-S nanorods.

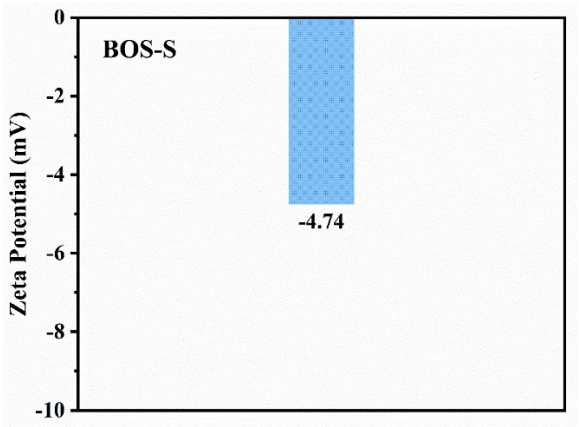

Fig. S3 Zeta potential of BOS-S.

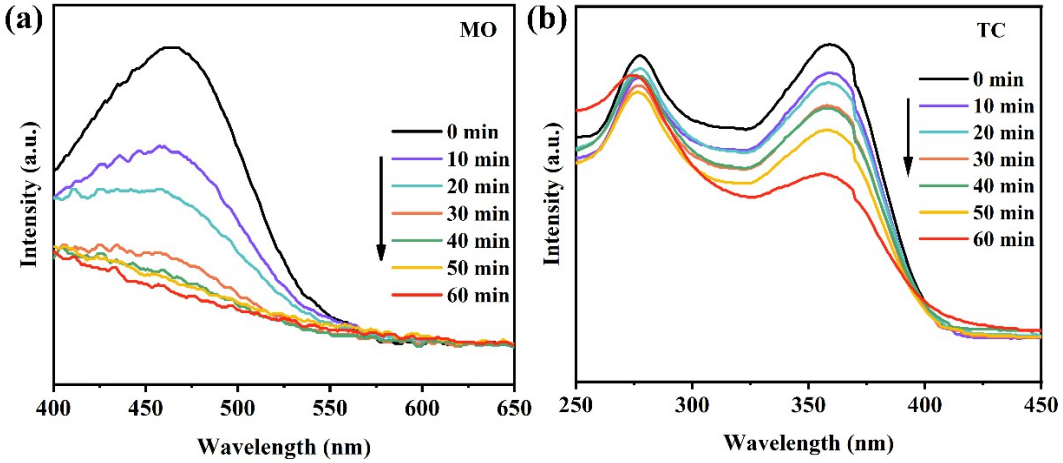

Fig. S4 UV-vis spectral change of (a) MO and (b) TC that piezoelectricity degraded by BOS-S.

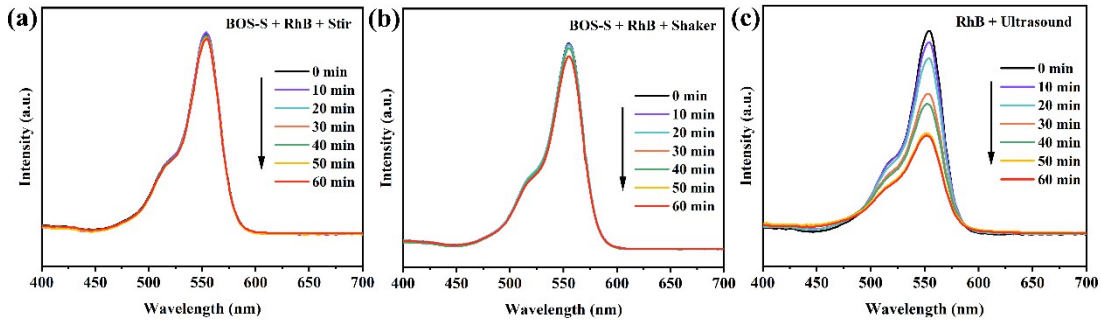

Fig. S5 (a) UV-vis spectral change of RhB under different conditions: (a) catalyst, dye and agitation, (b) catalyst, dye and shaker, (c) dye and ultrasound.

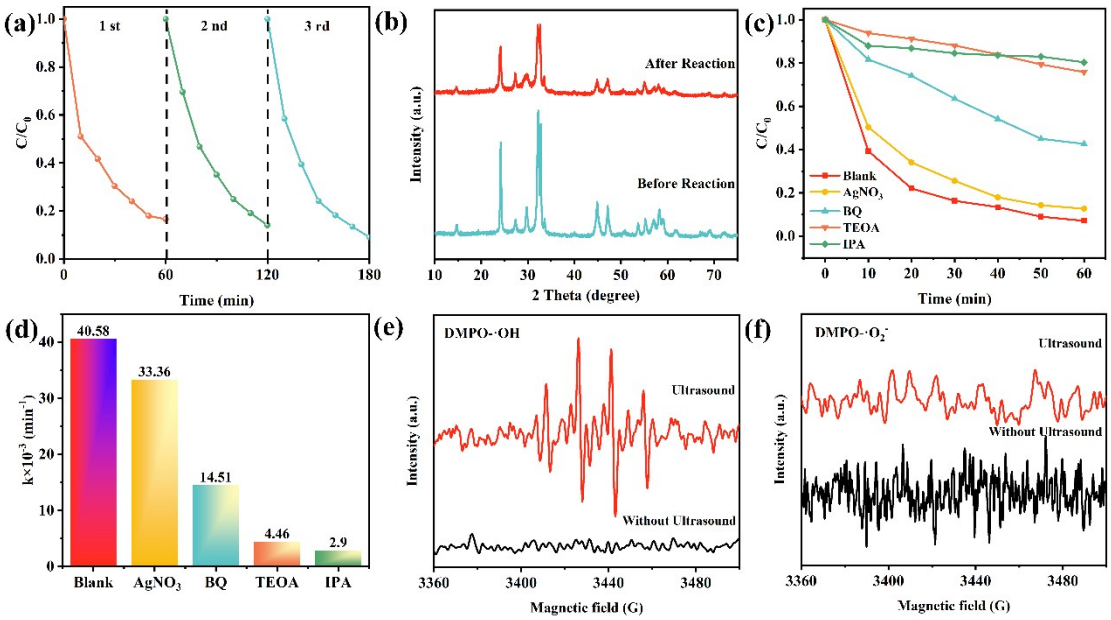

Fig. S6 (a) Recycling measurements and (b) the XRD patten of before and after piezo catalytic of RhB for BOS-S, (c) piezoelectric-catalyzed degradation of RhB dye by BOS-S in the presence of different radical scavengers, (d) kinetic rate constants of the reaction of BOS-S with different radical scavengers, (e) DMPO-·OH ESR spectra of BOS-S in aqueous dispersions, (f) DMPO-·O_2^- ESR spectra of BOS-S in MeOH dispersions

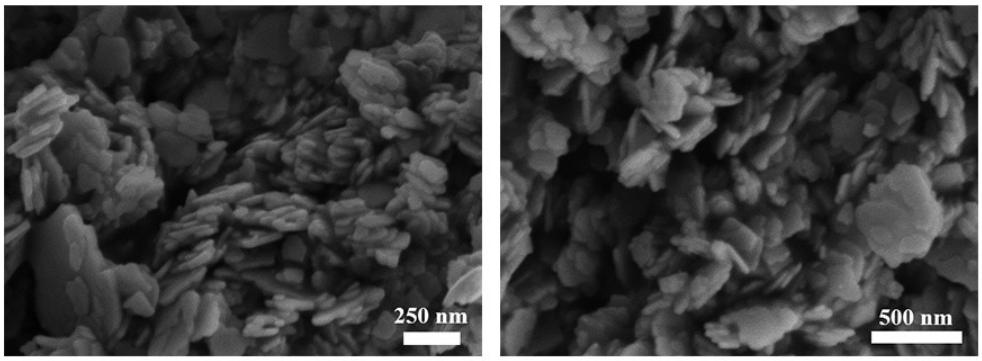

.

Fig. S7. The SEM of the BOS-S after cycling.

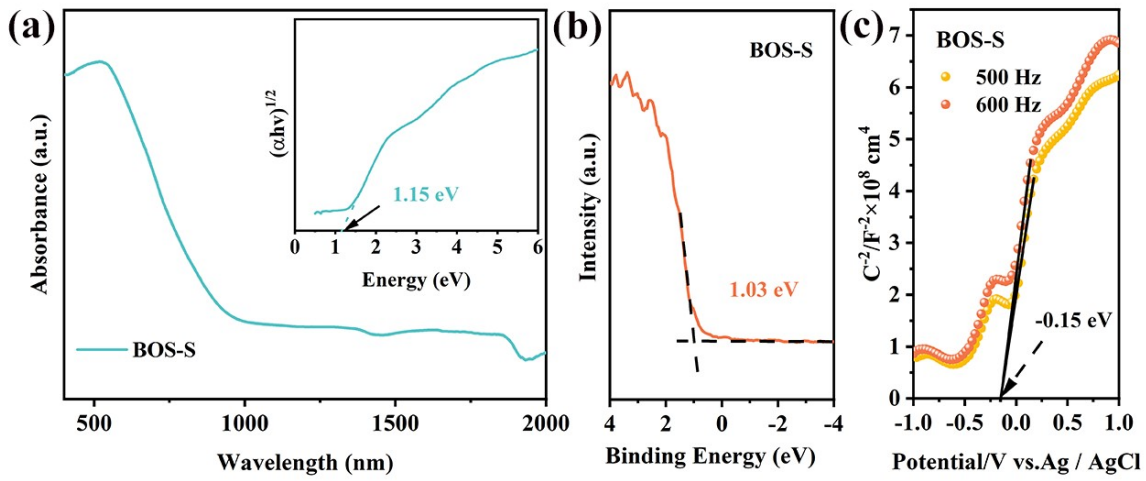

Fig. S8 (a) UV-visible diffuse reflection spectrum (the insert is the relationship between $(\alpha hv)^{1/2}$ and light energy (hv)), (b) XPS valence band spectrum and (c) Mott-Schottky curve of BOS-S sample.

The BOS-S sample presents a wide light absorption range from ultraviolet to visible then to near-infrared in Fig. S8a. The band-gap width of BOS-S is 1.15 eV through the fitting calculation of equation (1-1), in which BOS-S is an indirect band-gap semiconductor material, and the n value is 1/2.[1] The XPS valence band of Fig. S8b shows a valence band potential (E_{VB}) of BOS-S is 1.03 eV. The conduction band potential of BOS-S is calculated to be -0.12 eV according to equation (1-2). To further determine the energy band structure of BOS-S, Mott-Schottky curve (MS) is obtained. A positive slope of the curve is observed from Fig. S8c, indicating that BOS-S is an n-type semiconductor.[2,3] The intercept of the MS curve on the X-axis is the flat-band potential (E_{fb}), the E_{fb} of BOS-S is -0.15 V (vs. Ag/AgCl). The E_{fb} ratio conduction band potential (E_{CB}) for n-type semiconductors is corrected (0.20 V), and the E_{CB} for calculating BOS-S is -0.35 V vs. Ag/AgCl. Through equation (1-3) conversion, the E_{CB} of BOS-S is -0.15 eV (vs. NHE), which is basically consistent with the calculation result of XPS valence band.

$$(\alpha hv)^n = k(hv - E_g) \quad (1\text{-}1)$$

$$E_{CB} = E_{VB} - E_g \quad (1\text{-}2)$$

$$E_{NHE} = E_{Ag/AgCl} + 0.197\ V \quad (1\text{-}3)$$

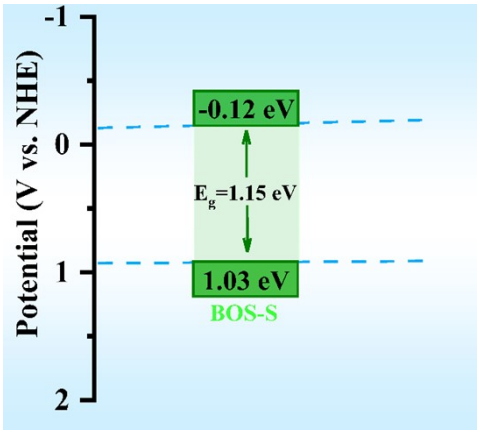

Fig. S9 The energy band gap structure of BOS-S.

Table S1. Comparison of the piezoelectric coefficient (d_{33}) of Bi_2O_2S with those of reported piezoelectric materials.

Piezocatalysts	**d_{33} (pm V^{-1})**	**reference**
Bi_2O_2S	29	This work
$MoSe_2$/PVDF	6.5	[4]
$BaTiO_3$/TCN	20.2	[5]
P-$KNbO_3$	10	[6]
$Sn_{0.97}Ag_{0.03}S_2$	4.5	[7]
$Bi_2Fe_4O_9$	4	[8]
MoS_2/Bi_2S_3	2.5	[9]
BFO MPL($BaTiO_3$)	18.6	[10]
$BiFeO_3$@CdS	4	[11]
In_2Se_3	1.6	[12]
$BaTiO_3$NFs	11.1	[13]
MoS_2/BP	14.3	[14]

Table S2. Comparison piezocatalytic degradation of organic pollutants performances over catalysts previously reported with this work.

Piezocatalysts	Dyes species and concentration	Conditions	Degradation efficiency	Reference
Bi_2O_2S	MB, 5 mg/L RhB, 5 mg/L	100 W, 40 kHz	92.8%, 60 min. 97.7%, 60 min.	This work
$Ba(Zr_{0.05}Ti_{0.95})O_3$	MB, 5 mg/L RhB, 5 mg/L	180 W, 40 kHz	90%, 90 min. 70%, 90 min.	[15]
Au−ZnO	RhB, 5 mg/L	80 W, 40 kHz	88%, 75 min.	[16]
$NaNbO_3$	RhB, 5 mg/L	50 W, 40 kHz	61.9%, 100 min.	[17]
ZIF-8	RhB, 5 mg/L	180 W, 40 kHz	94%, 150 min.	[18]
$BiVO_4$	MB, 5 mg/L	150 W, 40 kHz	86.4%, 40 min.	[19]
Ag/LN-PVDF	RhB, 5 mg/L MB, 5 mg/L	70 W, 40 kHz	80%, 120 min. 89%, 120 min.	[20]
$Pb(Zr_{0.52}Ti_{0.48})O_3$	MB, 5 mg/L	70 W, 40 kHz	84%, 120 min.	[21]
CuS/ZnO	MB, 10 mg/L	150 W, 40 kHz	94.7%, 40 min.	[22]
$BaTiO_3$	MB, 5 mg/L	120 W, 40 kHz	77.0%, 60 min.	[23]

References

1 V. Cilamkoti, R.-K. Dutta, *Adv. Sustainable Syst.*, 2024, 2400034.

2 L.-S. Jiang, Z.-Y. Li, D.-Y. Wang, T.-Guo, and Y. Hu, *Appl. Surf. Sci.*, 2022, 601, 154185.

3 Y.-H. Wu, J.-S. Liu, J. Rong, Y.-Z. Zhang, Q. Liang, M. Zhou, Z.-Y. Li, and S. Xu, *Appl. Surf. Sci.*, 2023, 620, 156781.

4. X.-P. Chen, A.-J. Li, L.-L. Xing, J.-P. Wang, Y.-R. Sun, Y.-F. Wang, G.-Q. Chen, T.-L. Xing, and L. Xu, *J. Water Process Eng.*, 2024, **59**, 105015.

5. S.-X. Gong, W.-X. Zhang, Z.-R. Liang, Y.-J. Zhang, T. Gan, H.-Y. Hu, and Z.-Q. Huang, *Chem. Eng. J.,* 2023, **461**, 141947.

6. R. Huang, W. Cai, H. Zhang, Z.-H. Wang, Q. Zhan, R.-L. Gao, G. Chen, X.-L. Deng, X. Lei, J.-L. Dong, X.-Y. Liu, and C.-L. Fu, *J. Environ, Chem. Eng.*, 2023, **11**, 110177.

7. W.-R. Tian, J. Han, L.-C. Wan, N.-J. Li, D.-Y. Chen, Q.-F. Xu, H. Li, and J.-M. Lu, *Nano. Energy*, 2023, **107**, 108165.

8. V. Tiron, R.-J. jie, I. Dumitru, N. Cimpoesu, I. Burducea, D. Iancu, A. Borhan, S. Gurlui, and G. Bulai, *Ceram. Int.*, 2023, **49**, 20304-20314.

9. J.-Y. Yue, R. Wu, Y. Zhang, N. Zhang, H.-T. Jing, S.-H. Wei, and F.-P. Ouyang, *Appl. Surf. Sci.*, 2023, **623**, 157033.

10. T.-N. Nguyen, K.-S. Chang, *J. Environ. Chem. Eng.*, 2022, **10**, 107213.

11. J.-J. Long, T.-T. Ren, J. Han, N.-J. Li, D.-Y. Chen, Q.-F. Xu, H. Li, and J.-M. Lu, *Sep. Purie. Technol.*, 2022, **290**, 120861.

12 J. Xu, W. Yang, S. Hu, X. Lai, and J. Jian, *J. Mater. Sci.*, 2022, **57**, 5072-5083.

13. D.-M. Liu, C.-C. Jin, F.-K. Shan, J.-J. He, and F. Wang, *ACS Appl. Mater. Interfaces*, 2020, **15**, 17443-17451.

14. M.-K. Mohanta, A. Rawat, N. Jena, Dimple, R. Ahammed, and A.-D. Sarkar, *ACS Appl. Mater. Interfaces*, 2019, **12**, 3114-3126.

15. M.-D. Zhu, S.-Q. Li, H.-F. Zhang, J. Gao, K.-W. Kwok, Y.-M. Jia, L.-B. Kong, W.-Y. Zhou, and B.-L. Peng, *Nano Energy*, 2021, **89**, 106474.

16. D.-L. Xiang, Z.-R. Liu, M.-Q. Wu, H.-H. Liu, X.-D. Zhang, Z. Wang, Z.-L. Wang, and L.-L. Li, *Small*, 2020, **16**, 1907603.
17. D. Fernandes，M.-M. Ferrer, C.-W. Raubach, M.-L. Moreira, L.-G. Jardim, E.-C. Moreira, F.-O. Graeff, and S.-S. Cava, *J. Am. Ceram. Soc.*, 2023, **106**, 399–409.
18. L.-J. Ruan, Y.-M. Jia, J.-F. Guan, B.-Xue, S.-H. Huang, Z. Wu, G.-R. Li, and X.-Z. Cui, *Sep. Purif. Technol.*, 2022, **28**, 3120159.
19. M. Kumar, I. Kebaili, R. Vaish, J.-E. Ghoul, and M.-U. Khandaker, *Mater. Today Commun.*, 2023, **37**, 107306.
20. G. Singh, M. Sharma, and R. Vaish, *ACS Appl. Mater. Interfaces*, 2021, **13**, 22914−22925.
21. S, Verma, M. Sharma, A. Halder, and R. Vaish, *Surf. Interfaces*, 2022, **30,** 101827.
22. X.-R. Ning, D.-Z. Jia, S.-H. Li, M.-F. Khan, and A.-Z. Hao, *Ceram. Int.*, 2023, **49**, 21658-21666.
23. A. Gaur, V.-S. Chauhan, and R. Vaish, *Environ. Sci. Adv.*, 2023, **2**, 462.